Down-regulation of GP130 signaling sensitizes bladder cancer to cisplatin by impairing Ku70 DNA repair signaling and promoting apoptosis

Shanshan He, MD[a,1,‡], Gang Li, PhD[a,2,‡], Andreas G. Schätzlein, PhD[b], Peter A. Humphrey, MD, PhD[c], Robert M. Weiss, MD[a], Ijeoma F. Uchegbu, PhD[b], and Darryl T. Martin, PhD[a,*].

[a]Department of Urology, Yale University, New Haven, CT; [b]School of Pharmacy, University College London, London, UK; and [c]Department of Pathology, Yale University, New Haven, CT.

Present Address: [1]Department of Breast Reconstruction, Tianjin Medical University Cancer Institute and Hospital, National Clinical Research Center for Cancer, Key Laboratory of Cancer Prevention and Therapy, Tianjin, China; [2]School of Pharmacy, University College London, London, UK.

[‡] These authors contributed equally to this work.

[*] To whom correspondence should be addressed.

Phone: 203.785.4195; Fax: 203.785.4043; email: darryl.martin@yale.edu

Short Title: GP130 and Ku70 in bladder cancer

Abstract

Chemoresistance is one of the barriers for the development of bladder cancer treatments. Previously, we showed that glycoprotein-130 (GP130) is overexpressed in chemoresistant bladder cancer cells and that knocking down GP130 expression reduced cell viability. In our current work, we showed that down-regulation of GP130 sensitized bladder cancer cells to cisplatin-based chemotherapy by activating DNA repair signaling. We performed immunohistochemistry and demonstrated a positive correlation between the levels of Ku70, an initiator of canonical non-homologous end joining repair (c-NHEJ) and suppressor of apoptosis, and GP130 in human bladder cancer specimens. GP130 knockdown by SC144, a small molecule inhibitor, in combination with cisplatin, increased the number of DNA lesions, specifically DNA double-stranded breaks, with a subsequent increase in apoptosis and reduced cell viability. Furthermore, GP130 inhibition attenuated Ku70 expression in bladder and breast cancer cells as well as in transformed kidney cells. In addition, we fabricated a novel polymer-lipid hybrid delivery system to facilitate GP130 siRNA delivery that had a similar efficiency when compared with Lipofectamine, but induced less toxicity.

Keywords

DNA repair, Apoptosis, Ku70, Glycoprotein 130, Hybrid nanoparticles

1. Introduction

The standard first-line therapy for muscle invasive bladder cancer is neoadjuvant cisplatin-based chemotherapy followed by surgery [1]. Despite an initial response, cisplatin-based treatments often result in a chemotherapy refractory state, and therapeutic failure [2]. Cisplatin (Cisp) is a DNA damaging agent that causes inter-strand and intra-strand DNA crosslinks [2]. Augmenting DNA damage responses to cancer treatments has been shown to sensitize cancer cells to cisplatin-based treatments [3-6]. Double strand breaks (DSBs) are among the most lethal types of DNA damage, which directly cause cell death if left unrepaired, or can result in genome instability if repaired incorrectly [7]. DSBs are repaired by homologous recombination (HR) or canonical non-homologous end joining (c-NHEJ), a primary repair pathway in mammals [7, 8]. Ku70 (also known as XRCC6), a key component in c-NHEJ, plays a pivotal role in DNA lesion recognition [9]. The binding of the Ku70/Ku80 heterodimer to broken DNA ends activates a DNA-dependent kinase complex, recruits other repair elements, and provides a central scaffold for the assembled repair complex [10, 11]. It has been shown that increases in Ku70 expression could lead to chemoresistance [12]. Therefore, Ku70 is a gatekeeper to c-NHEJ initiation.

The interleukin 6 (IL-6) family of cytokines is upregulated in many cancers such as breast, lung, and bladder cancer [13-15], and this increase correlates with poor prognosis [16]. We previously demonstrated that glycoprotein 130 (GP130), a signal transducer for IL-6 family cytokines, was highly expressed in aggressive bladder cancer, and that silencing GP130 decreased tumor size by 70 % in a bladder cancer xenograft mouse model [17]. There is growing evidence that IL-6/GP130 signaling plays a role in the DNA damage response in human colorectal and lung cancers [18-20]; however, its role in bladder cancer is unclear. Therefore, we hypothesized that inhibiting the glycoprotein signaling pathway will sensitize muscle invasive bladder cancer cells to cisplatin and that this may involve alterations in Ku70.

Obstacles in treating bladder tumors with intravesical instillations include short drug exposure due to voiding, low penetration of the bladder permeability barrier, and potential cytotoxicity [21, 22]. Therefore, we were interested in developing a system that could avoid the above caveats. Hence, we developed a delivery system for GP130 siRNA that has the potential to reduce vehicle toxicity, while improving gene-based drug bioavailability. We delivered GP130 siRNA with novel positively charged chitosan-lipid hybrid nanoparticles (EGCDNPs) consisting of the chitosan derivative, [*N*-(2-ethylamino)-6-*O*-glycolchitosan] (EAGC) and 1,2-dioleoyl-sn-glycero-3-phosphoethanolamine (DOPE) lipid that had been demonstrated to have mucoadhesive properties, to be biocompatible, and to effect gene transfer in *in vitro* bladder cells and in *in vivo* murine bladder models [23] [GL unpublished data]. The use of nanomedicine for altering cancer cell signaling will improve bioavailability and lead to better non-viral treatment options of bladder cancer.

2. Materials and methods

Patient tissue specimens: Thirty-nine deidentified specimens were collected from 30 patients who underwent transurethral resection of bladder tumor (TURBT) or cystectomy. The specimens were comprised of 39 low- and high-grade bladder cancers that were graded by a genitourinary pathologist using WHO 2016 criteria [24]. Two adjacent normal bladder specimens were used as negative controls. Paraffin-embedded sections were obtained from the Yale Genitourinary Biospecimen Repository, the Yale Pathology Tissue Services (YPTS), and US BioMax, Inc. The Yale tissue microarray (TMA) was constructed using 1.0 mm cores and the BioMax TMA was constructed using 1.5 mm cores. All patients provided informed consent and were offered enrollment into a biospecimen repository approved by the Yale University Institutional Review Board.

Immunohistochemistry: Immunohistochemistry was carried out on formalin fixed, paraffin-embedded (FFPE) TMAs as previously described (16). In brief, the paraffin-embedded sections

were deparaffinized in xylene and rehydrated with graded ethanol before undergoing heat-induced antigen retrieval. GP130 antibody (NBP2-15776, Novus Biologicals), Ku70 antibody (A-9, Cell Signaling) or no antibody (negative control) were used before being developed using a DAB (3,3'-diaminobenzidine) substrate kit, and counterstained with hematoxylin. Paraffin-embedded human UM-UC-3 cell pellets were used as positive controls. GP130 and Ku70 staining intensity was evaluated using 0, no signal; 1+, light brown on high magnification (400X); 3+, dark brown on low magnification (100X); or 2+, between low and high signal. A blind staining evaluation was performed by SH and DTM before the pathological grading was revealed.

Cell lines and reagents: Human invasive bladder cancer cells UM-UC-3 and TCCSUP, were purchased from American Type Culture Collection, and breast cancer cells (MCF-7) and transformed embryonic kidney cells (HEK-293T) were gifts from Drs. Elias Theodorou and Brian Shuch, respectively. The derived drug resistant UM-UC-3 (UM-UC-3R) cells were established by continuous exposure to gemcitabine and cisplatin [25]. UM-UC-3, UM-UC-3R, and TCCSUP cells were cultured with Minimum Essential Medium Eagle (MEME) (Sigma-Aldrich), whereas MCF-7 and HEK-293T cells were cultured with Dulbecco's Modified Eagle's Medium (DMEM; Corning). All cells were supplemented with 10 % fetal bovine serum (FBS) (Sigma Aldrich), 1 % glutamine and placed in a humidified atmosphere containing 5 % CO_2 in air. Prior to the start of the experiments, all cells were reauthenticated for quality control using short tandem repeat DNA profiles (The Yale University DNA Analysis Facility, New Haven, CT). In addition, all cells were routinely tested for mycoplasma (MycoAlert™, Lonza Biologics Inc.). UM-UC-3 and UM-UC-3R cells were treated with 3.5 µM SC144 (GP130 inhibitor; Sigma Aldrich) for 24 h followed by 48 h incubation with cisplatin (Santa Cruz) at concentrations of 0.3 µg/mL and 11.2 µg/mL, respectively. TCCSUP, MCF-7, and HEK-293T, cells were treated with 5 µM SC144 for 24 h followed by 48 h recovery.

Crystal Violet staining: To analyze cell survival, crystal violet was applied with a modified protocol as previously described [17]. Briefly, adherent cells were washed with PBS and fixed with 4 % paraformaldehyde for 10 mins, stained with 0.5 % crystal violet dye for 10 mins, and washed with dH_2O thrice for 5 mins. Images were acquired with a biological microscope (Olympus), and viable cells were counted and recorded.

Alkaline Comet Assay: DNA strand breaks were evaluated by an alkaline single cell gel electrophoresis assay. The comet assay was performed according to the manufacturer's protocol (Trevigen). Briefly, after specific treatments, cells were mixed with low melting point agarose, lysed, and DNA unwinding was performed before undergoing electrophoresis. For positive controls, UM-UC-3/UM-UC-3R cells were treated with 100 µM H_2O_2 for 20 min at 4 °C, as recommended by the manufacturer's instructions (Trevigen, USA). Strand breaks cause increased migration of DNA and form a comet-like shape after electrophoresis. Slides were neutralized, fixed, and stained with SYBR™ Safe (Invitrogen) before images were acquired with a fluorescent microscope (Zeiss Axio Observer Z1). At least 100 randomly selected nuclei were analyzed for tail percent DNA on each treatment using Comet Score analysis (TriTek Corp). Percent DNA in tails was calculated by total intensity of tail divided by total intensity of comet × 100 %.

Western Blot: Proteins were quantified using the Bradford Protein Assay (Bio-Rad, Laboratories, Inc., CA, USA) before being separated on SDS-PAGE gels and transferred to PVDF membranes. Primary antibodies were used against GP130 (NBP2-15776, Novus Biologicals), γH2AX (p-Ser 139), Ku70 (A-9), vinculin (7F9) (Santa Cruz), cleaved caspase-3 (D175), p-ATM (S1981), beta-actin (13E5), and GAPDH (14C10) (Cell Signaling). A chemiluminescence system (Thermo Scientific, Rockford IL) was used to detect protein signal. Samples were normalized based on

house-keeping protein quantification, and band density was determined using ImageJ software (NIH) [17].

Nanoparticle material and synthesis: [*N*-(2-ethylamino)-6-*O*-glycolchitosan)] EAGC (Mw = 83.0 kDa, polydispersity indices (PDI) = 1.016) was previously synthesized with an ethylamino mole substitution of 28.0 % (GL unpublished data). DOPE lipid (1, 2-dioleoyl-sn-glycero-3-phosphoethanolamine) was purchased from Avanti Polar Lipids, Inc. (Alabaster, AL, USA).

Characterization of EAGC-DOPE lipid hybrid nanoparticles (EGCDNPs) loaded with GP130 siRNA (siGP130)

(i) Preparation of EGCDNPs and siGP130 – EGCDNPs complexes

The film evaporation technique was employed to fabricate EAGC-DOPE hybrid nanoparticles (EGCDNPs). Briefly, chloroform solution containing DOPE lipid (1 mL, 2 mg/mL) was placed on a rotary evaporator for 20 min under reduced pressure to remove the solvent and form a thin film. EAGC solution [1 mL, 2 mg/mL in 2 mM phosphate buffer (PB), pH = 6] was then added to form the EGCDNPs under vigorous vortex. The siRNA (in RNase free water) was complexed with EGCDNPs in PB buffer (2 mM, pH = 6) at EGCDNPs, siRNA mass ratios of 1:1, 5:1 or 20:1 (siRNA final concentration of 8 µg/mL). The complexes were allowed to incubate at room temperature (RT) for 75 mins before use.

(ii) Dye exclusion assay

To assess the siRNA binding, EGCDNPs – siRNA complexes (containing 8 µg/mL of siRNA, 80 µL) at EGCDNPs, siRNA mass ratios of 1:1, 5:1 and 20:1 (F_0) or naked siRNA controls (F_t) were added into wells of a 96-well microplate followed by incubation with equal volumes of PicoGreen solution (80 µL in 2 mM PB buffer, pH = 6). The fluorescence of free siRNA was determined by exciting the complex with Picogreen at 485 nm and reading the fluorescence at 520 nm under a

fluorescence plate reader (PHERAstar, BMG Labtech). The fluorescence values were normalized to wells containing only siRNA and PicoGreen (F_t - F_o / F_t).

(iii) Size, zeta potential, and stability of siGP130 – EGCDNPs/EGCDNPs

siGP130 **–** EGCDNPs complexes or EGCDNPs alone were characterized by assessing their size, surface charge, and morphology. Size was measured by Dynamic Light Scattering (DLS, Nano ZS, Malvern) using a He-Ne laser at 633 nm of wavelength. The zeta potential of the NPs was measured by Zetasizer Nano ZS (Malvern). To check the *in vitro* stability of polymer-lipid siRNA NPs, the siRNA NPs were stored at 4 °C for two days and their particle size, zeta potential and PDI measured. The above-mentioned naked GP130 siRNA and EGCDNPs-siGP130 complexes also were subjected to electrophoresis (60 V for 40 min) in a 4 % (w/v) agarose gel, stained with SYBR™ Safe. The results were imaged on a ChemiDoc™ MP System (Bio Rad) to visualise the SYBR™ Safe – stained free siRNA in the gels. Last, for TEM (Transmission Electron Microscopy), EGCDNPs loaded with siGP130 were stained with 1 % uranyl acetate and imaged using a JEOL 1400 Plus microscope (JEOL Ltd).

siRNA transfection: For RNA interference, UM-UC-3 and UM-UC-3R cells were transfected with a pre-designed siGP130 sequence [17], and with a scrambled sequence (siSC) control (universal negative control#1) in a six well plate using Lipofectamine RNAiMAX Transfection Reagent (Invitrogen) (4 µg GP130/well) as well as EAGC-DOPE lipid hybrid nanoparticles (EGCDNPs) (4 µg GP130 siRNA/well). siGP130 and siSC were purchased from Sigma-Aldrich.

Cell viability of bladder cancer cells upon the treatment of EGCDNPs: Briefly, human bladder cancer cell lines (UM-UC-3, UM-UC-3R) were seeded at a density of 5×10^3 cells per well in a 96 well plate followed by 24 h of recovery. EGCDNPs/Lipofectamine 2000 were applied to the cells for a duration of 6 h, after which the treatments were removed and replenished with fresh medium

for a further 48 h recovery. The cell viability of EGCDNPs- and Lipofectamine 2000-treated cells was evaluated using the WST-1 assay (Clontech Laboratories) as previously described [26].

Statistical analysis: Data are expressed as mean ± SEM based on three to six independent experiments unless otherwise noted. Data were analyzed using Student's *t*-test, one-way or two-way ANOVA with post hoc comparison, where appropriate. Categorical variables were analyzed by Chi square test. All statistical tests were considered to be statistically significant in which * represents $p < 0.05$, ** represents $p < 0.01$, *** represents $p < 0.001$, and **** represents $p < 0.0001$ unless indicated differently. Statistical analysis was carried out using the GraphPad Prism 8.0 (GraphPad Software, Inc).

3. Results

3.1 GP130 and Ku70 expression in bladder cancer tissue microarrays (TMAs) and whole bladder sections.

Immunohistochemistry was performed on TMAs to assess GP130 and Ku70 expression in bladder cancer specimens (Fig. 1A). Thirty-seven out of 39 bladder cancer TMA specimens (95 %) were both GP130 and Ku70 positive (Fig. 1B) whereas minimal expression of GP130 and Ku70 was found in normal bladder tissues (Fig. S1). A strong association was found between GP130 and Ku70 staining intensity (Fig. 1B, $p < 0.0001$). In addition, we found a significant correlation between bladder cancer grades and GP130 levels ($p < 0.05$; Fig. 1C), whereas a significant correlation was not found between bladder cancer grade and Ku70 levels ($p = 0.068$; Fig. 1D).

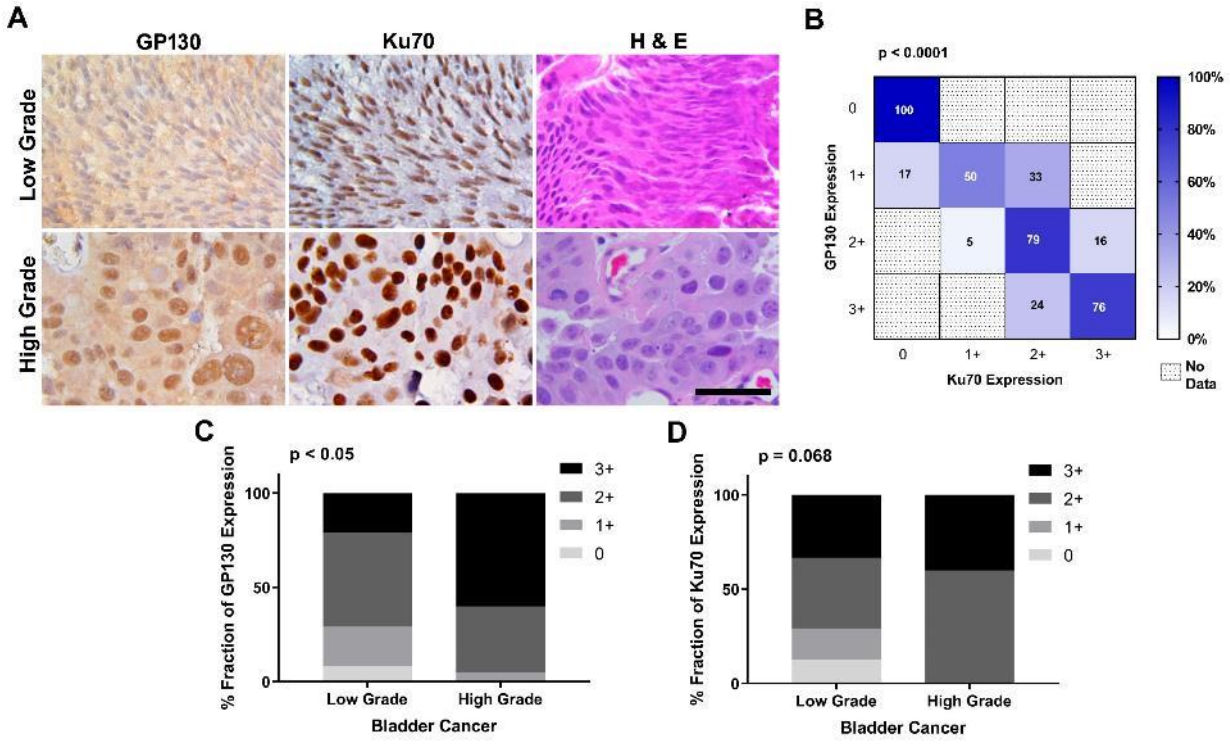

Fig. 1. GP130 and Ku70 levels of expression in human bladder cancer specimens. Immunohistochemistry was performed on low- and high-grade bladder cancer specimens for GP130 and Ku70. Representative IHC and H & E staining are shown (A). The number in each box represents the percent correlation between GP130 (y-axis) and Ku70 (x-axis) for a particular staining intensity (B). The staining intensity (0, 1+, 2+, or 3+) of GP130 and Ku70 were fractionated based on tumor grade (C, D). Scale bars = 5 µm.

3.2 Reduced cell growth upon SC144 and cisplatin treatment of invasive bladder cancer cells.

To investigate if a combination of GP130 inhibition and a DNA damaging agent will have a synergistic effect on cell growth, we treated UM-UC-3 and UM-UC-3R bladder cancer cells with SC144 and cisplatin. UM-UC-3R cells previously have been shown to be more aggressive than UM-UC-3 cells [25]. Crystal violet staining demonstrated that the combination of cisplatin and SC144 reduced cell growth more effectively than SC144 or cisplatin treatment, alone (Fig. 2A, C). In UM-UC-3 cells, a combination of SC144 and cisplatin significantly decreased the number of

cells compared to a single treatment with either SC144 (by 39.10 ± 9.13 %, $p < 0.05$) or cisplatin (by 42.61 ± 9.13 %, $p < 0.01$) alone (Fig. 2B). Similarly, a combination of SC144 and cisplatin significantly decreased the number of drug-resistant UM-UC-3R cells compared to a single treatment of SC144 (by 33.36 ± 3.58 %, $p < 0.0001$) or cisplatin (by 19.22 ± 3.58 %, $p < 0.01$) alone (Fig. 2D).

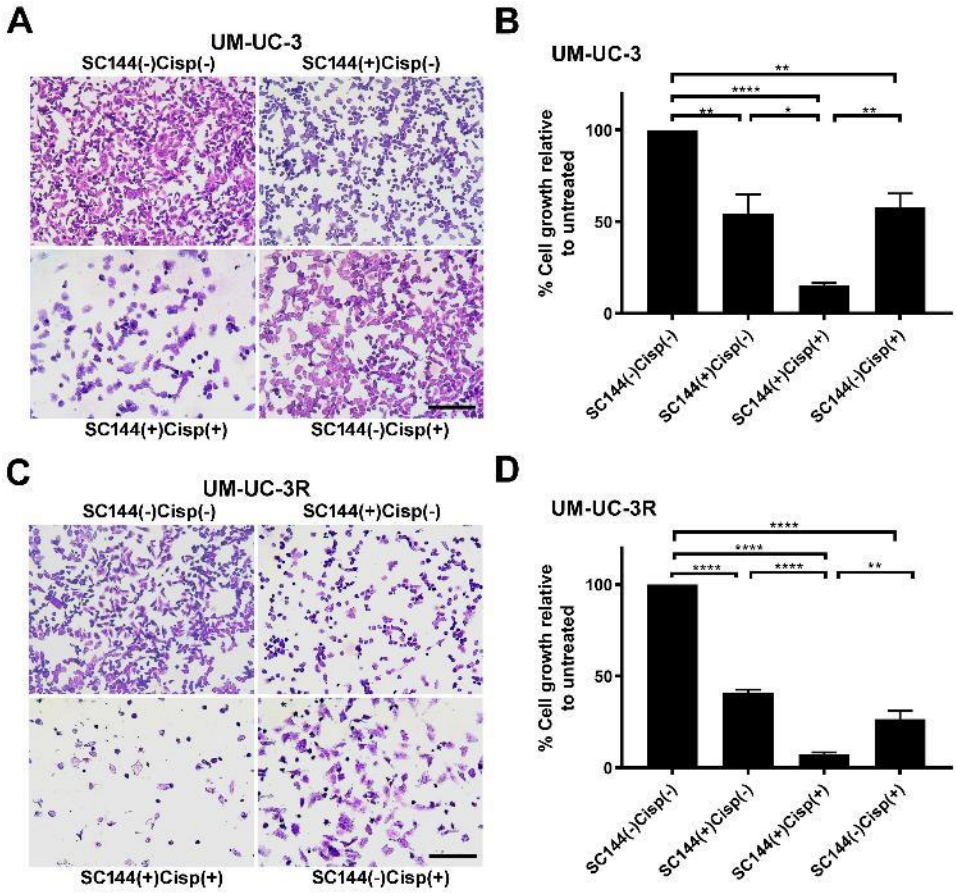

Fig. 2. GP130 inhibition sensitized invasive bladder cancer cells to cisplatin treatment and reduced cell viability. UM-UC-3 (A, B) and UM-UC-3R (C, D) cells were treated with SC144 for 24 h followed by 48 h incubation in cisplatin (Cisp) at 0.3 µg/mL and 11.2 µg/mL, respectively. Representative crystal violet staining shows cell morphology in UM-UC-3 (A) and UM-UC-3R (C) bladder cancer cells. Quantification of inhibitory effects of SC144, cisplatin, or a combination of cisplatin and SC144 on cell growth in UM-UC-3 (B) and UM-UC-3R (D) bladder cancer cells. Scale bars = 100 µm. * represents $p < 0.05$, ** represents $p < 0.01$, and **** $p < 0.0001$.

3.3 Inhibition of GP130 expression by SC144 sensitizes bladder cancer cells to cisplatin by inducing DNA lesions, down-regulating Ku70 expression, and promoting apoptosis.

To investigate whether the synergistic effect of SC144 and cisplatin had an impact on DNA damage, an alkaline comet assay was performed. In UM-UC-3 cells, a shift towards a higher percent tail DNA was observed in the co-treatment group (14.06 ± 1.00 %) compared to untreated controls (5.26 ± 0.50 %, $p < 0.0001$), SC144 treatment alone (6.25 ± 0.47 %, $p < 0.0001$) or cisplatin treatment alone (8.16 ± 0.77 %, $p < 0.0001$) groups (Fig. 3A, B). A higher percentage of tail DNA also was observed in UM-UC-3R cells with co-treatment (52.05 ± 2.58 %) when compared to untreated controls (8.91 ± 1.31 %, $p < 0.0001$), SC144 treatment alone (12.78 ± 1.48 %, $p < 0.0001$) or cisplatin treatment alone (19.39 ± 1.61 %, $p < 0.0001$) groups (Fig. 3C, D).

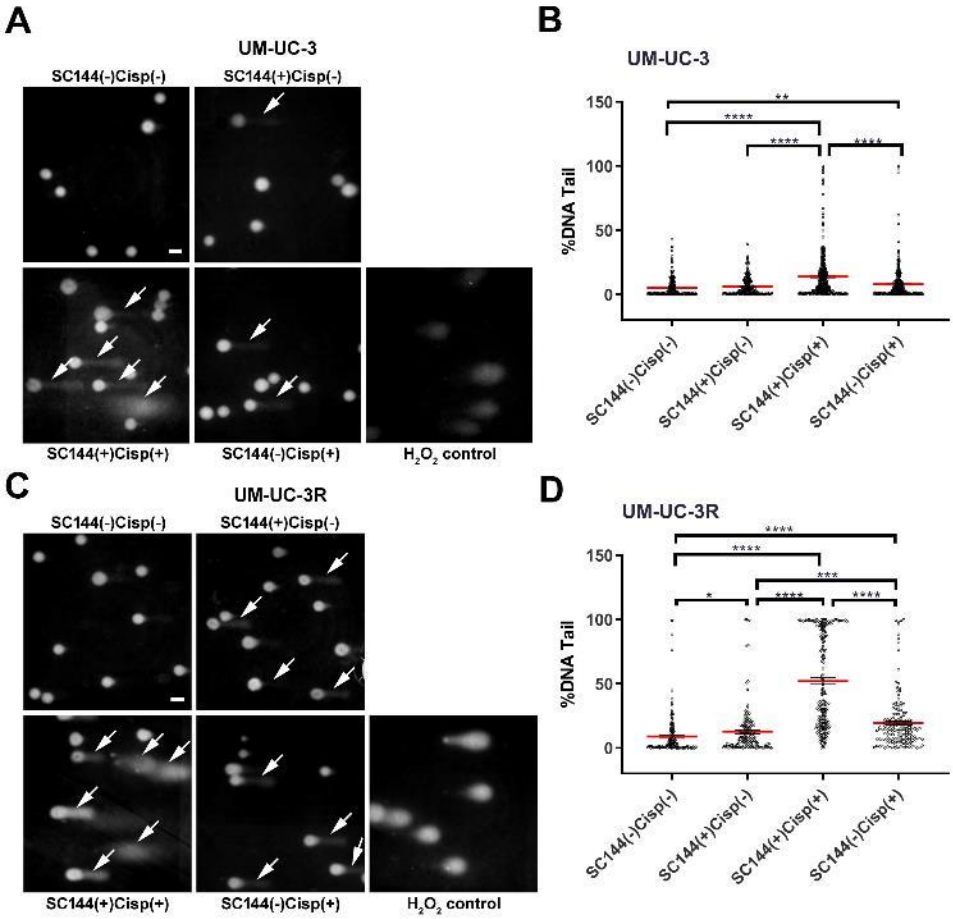

Fig. 3. Co-treatment with SC144 followed by cisplatin produced more DNA lesions than SC144 or cisplatin, alone in UM-UC-3 and UM-UC-3R cells. Alkaline single cell electrophoresis was performed to determine DNA strand breaks. Representative images are shown to illustrate the length of the comet tails in response to treatment (A, C). Scale bars = 50 µm. Quantification of mean tail moments from an average of more than 100 randomly selected nuclei are shown (B, D). Dunn's multiple comparisons test was performed. Data are shown as mean ± SEM. * represents $p < 0.05$, ** represents $p < 0.01$, *** represents $p < 0.001$, and **** $p < 0.0001$.

The effectiveness of GP130 down-regulation by SC144 treatment also was examined. SC144 knocked down GP130 levels in UM-UC-3 and UM-UC-3R cells by 54.01 ± 13.60 % ($p < 0.01$) and 48.75 ± 12.99 % ($p < 0.01$), respectively whereas cisplatin treatment alone did not significantly impact GP130 levels (Fig. 4A, 4B). Upon co-treatment with SC144 and cisplatin, GP130 levels decreased by 61.15 ± 13.60 % ($p < 0.01$), and 53.43 ± 12.99 % ($p < 0.01$), in UM-UC-3 and UM-

UC-3R, respectively (Fig. 4A, 4B). With respect to phosphorylated ataxia-telangiectasia mutated (pATM) levels (a key DNA damage response marker [27]), a significant increase was observed in UM-UC-3 cells with SC144 and cisplatin co-treatment compared with cisplatin (72.87 ± 10.72 %, $p < 0.001$) or SC144 (67.75 ± 10.72 %, $p < 0.01$), alone (Fig. 4A, 4C). Also, pATM was significantly increased in UM-UC-3R cells with SC144 and cisplatin co-treatment compared with SC144 (79.10 ± 15.60 %, $p < 0.01$), but not cisplatin alone ($p = 0.21$) (Fig. 4A, 4C). To further detect the DNA damage level, we performed western blots to determine γH2AX levels (a key marker for double strand breaks [28]) (Fig. 4A, 4D). In UM-UC-3 cells co-treatment with SC144 and cisplatin resulted in an upregulation of γH2AX expression, by 87.67 ± 6.51 % ($p < 0.0001$), 70.54 ± 6.51 % ($p < 0.0001$), and 67.75 ± 6.51 % ($p < 0.0001$) when compared to untreated controls, SC144 treatment alone, or cisplatin treatment alone, respectively (Fig. 4A, 4D). The γH2AX expression in the co-treatment group in UM-UC-3R cells was increased by 87.56 ± 8.71 % ($p < 0.0001$), 77.33 ± 8.71 % ($p < 0.0001$), and 29.53 ± 8.71 % ($p < 0.05$) compared with untreated controls, SC144 treatment alone, or cisplatin treatment alone, respectively (Fig. 4A, 4D).

To further define how GP130 inhibition may affect DSB DNA repair, we investigated the expression of Ku70, a key initiator protein in c-NHEJ DNA repair [9], by western blot analysis (Fig. 4A, 4E). In UM-UC-3 and UM-UC-3R cells, a significant down-regulation of Ku70 by 49.23 ± 10.62 %, $p < 0.01$ and by 29.94 ± 4.95 %, $p < 0.001$, respectively was observed 48 h after SC144 treatment (Fig. 4A, 4E). Co-treatment with SC144 and the DNA damaging agent cisplatin, resulted in a significant down-regulation of Ku70 in both UM-UC-3 cells by 43.41 ± 10.62 %, $p < 0.01$ and UM-UC-3R cells by 43.41 ± 4.95 %, $p < 0.0001$ (Fig. 4A, 4E). The level of apoptotic signaling, cleaved caspase-3, was increased upon co-treatment of cisplatin and SC144 compared to either cisplatin or SC144 treatment alone in UM-UC-3 cells by 74.73 ± 7.31 %, $p < 0.0001$ and by 90.86 ± 7.31 %, $p < 0.0001$, respectively, and in UM-UC-3R cells by 65.84 ± 13.14 %, $p < 0.01$ and by

83.37 ± 13.14 %, p < 0.001, respectively (Fig. 4A, 4F). SC144 treatment alone did not increase cleaved caspase-3 levels.

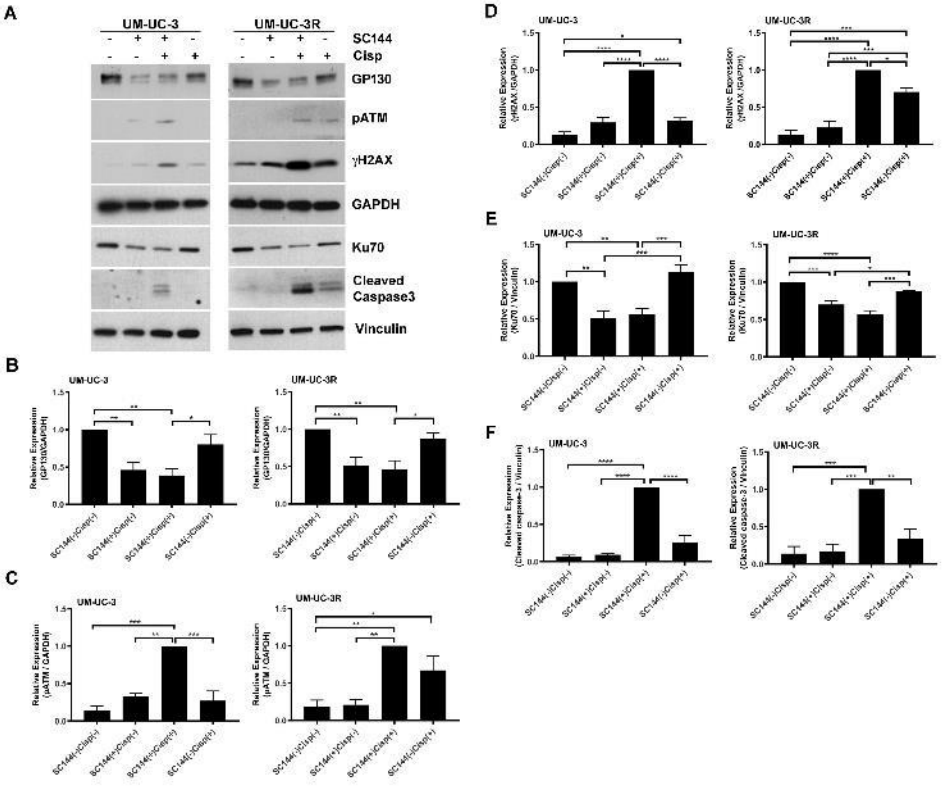

Fig. 4. Inhibition of GP130 by SC144 attenuates Ku70 expression and promotes apoptosis in the presence of a DNA damaging agent. UM-UC-3 and UM-UC-3R cells were untreated, treated with SC144 alone, SC144 followed by cisplatin (Cisp), or cisplatin alone. Representative western blots are shown to illustrate protein levels of GP130, pATM, γH2AX, Ku70, and cleaved-caspase3 (A). Protein levels were quantified for UM-UC-3 and UM-UC-3R cells (B–F). GAPDH and vinculin were used to show loading equivalency and protein integrity. Data are shown as mean ± SEM. * represents p < 0.05, ** represents p < 0.01, *** represents p < 0.001, and **** p < 0.0001.

We next determined if the association between GP130 signaling and the down-regulation of Ku70 expression was cell line specific by western blot analysis (Fig. 5A). We used three additional cell lines, TCCSUP, a human muscle invasive bladder cancer cell line, MCF-7, a human hormone

positive breast cancer cell line, and HEK-293T, a transformed embryonic human kidney epithelial cell line. We found similar associations between GP130 inhibition with SC144 (Fig. 5B) and Ku70 down-regulation with SC144 in all three cell types (Fig. 5C). SC144 decreased GP130 levels in TCCSUP, MCF-7, and HEK-293T cells (27.08 ± 7.26 %, $p < 0.05$; 53.96 ± 3.79 %, $p < 0.01$; and 50.29 ± 3.87 %, $p < 0.01$, respectively) and Ku70 levels in TCCSUP, MCF-7, and HEK-293T cells (34.01 ± 8.31 %, $p < 0.01$; 29.46 ± 6.80 %, $p < 0.01$; and 35.13 ± 11.19 %, $p < 0.05$, respectively).

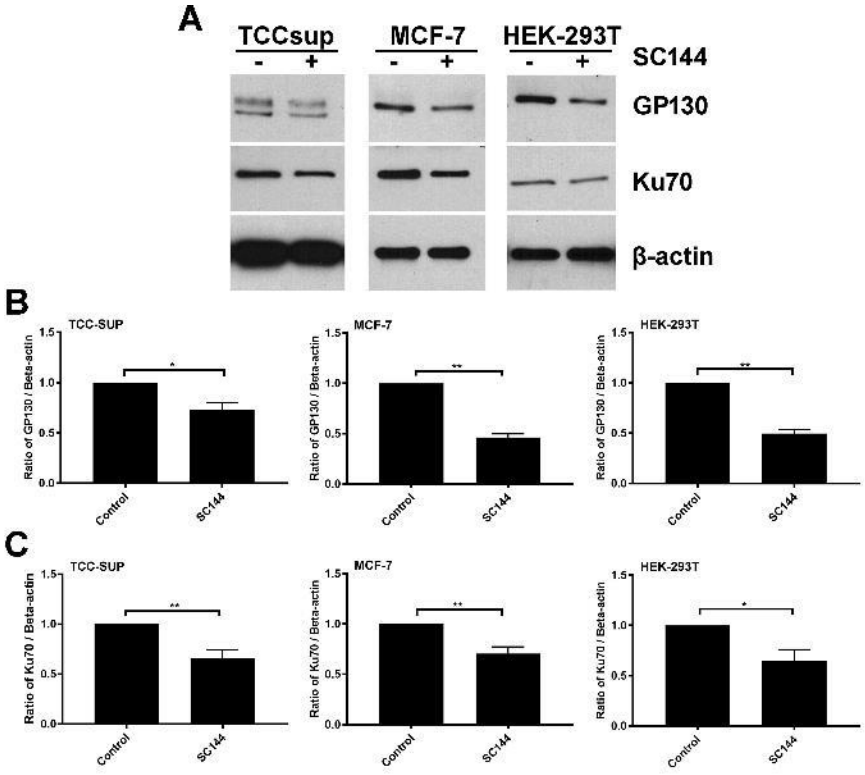

Fig. 5. GP130 inhibition by SC144 attenuates Ku70 expression. TCCSUP, MCF-7, and HEK-293T cells were treated with SC144 for 24 h and recovered for 48 h. GP130 and Ku70 expression was assessed by western blot (A) and quantified for GP130 (B) and Ku70 (C). GP130 protein levels were measured and normalized against beta-actin. Data are shown as mean ± SEM. * represents $p < 0.05$, and ** represents $p < 0.01$.

3.4 A novel cationic EGCDNPs that encapsulated GP130 siRNA facilitated the down regulation of GP130 signaling while decreasing cytotoxicity.

To seek out the ratio that can form a stable complex between EGCDNPs and siGP130 we tested EGCDNPs:siGP130 at mass ratios of 1:1, 5:1 and 20:1 by using PicoGreen dye exclusion and gel retardation assays. PicoGreen fluorescence increases significantly (~ 230-fold) on intercalation with GP130 siRNA compared to unbound (or free) PicoGreen. The electrostatic interaction between the anionic siRNA and the cationic EGCDNPs on formation of the complex condenses the siRNA and reduces the number of PicoGreen binding sites, ultimately reducing the fluorescence intensity of the PicoGreen solution. EGCDNPs:siRNA mass ratios of 5:1 and 20:1 significantly bound more siRNA when compared to an EGCDNPs:siRNA mass ratio of 1:1 ($p < 0.0001$; Fig. 6A). Although no binding difference was observed with the EGCDNPs:siRNA mass ratios of 5:1 and 20:1, data from the agarose gel electrophoresis experiment showed that at an EGCDNPs:siRNA mass ratio of 20:1, EGCDNPs could more effectively complex siGP130 compared to the corresponding 5:1 ratio (Fig. 6B). Based on these observations, EGCDNPs:siGP130 with a mass ratio of 20:1 was used for further studies. EGCDNPs alone presented as positive charged (+ 23.5 mV) NPs with a mean size of 278 ± 52 nm; EGCDNPs, siRNA at a mass ratio of 20:1, were positively charged complexes with a mean size of 184 ± 5 nm (Fig. 6C, E, F). No significant differences of size and PDI for the complex were observed when compared to EGCDNPs alone (Fig. 6E, F) at day 0. However, the zeta potential of the EGCDNPs alone was significantly more positive than that of the complex, indicating that the complexation of the cationic charge of the EGCDNPs and the anionic charge of the siRNAs effectively neutralizes the positive charge of the EGCDNPs (Fig. 6F; $p < 0.0001$). Over a two-day period, the EGCDNPs complex maintains a positive charge (Fig. 6G, $p < 0.01$).

EGCDNPs alone were stable over two days and had no appreciable change in size and zeta potential (Fig. 6E–G). Meanwhile, there was no difference in the PDI for the complex at day 0 and day 2, indicating that EGCDNPs form a stable complex with anionic siGP130 (Fig. 6F, G). Likewise, the gel electrophoresis (Fig. 6B, D) indicated that EGCDNPs – siRNA complexed at an

EGCDNPs, siRNA mass ratio of 20:1 was stable over two days without leaking free siRNA, corroborating the result obtained in single peak distribution (Fig. 6C). Additionally, using TEM we showed that at an EGCDNPs:siRNA mass ratio of 20:1, EGCDNPs interact with anionic siGP130 to form condensed and spherical particles (Fig. 6H).

EGCDNPs alone were significantly less toxic than Lipofectamine alone in both UM-UC-3 and UM-UC-3R cell lines (Fig. 7A–B, $p < 0.001$). EGCDNPs maintained over 85 % and 99 % cell viability in UM-UC-3 and UM-UC-3R cells, respectively, at the IC_{50} of Lipofectamine 3.71 µg/mL (UM-UC-3) and 2.51 µg/mL (UM-UC-3R). We then confirmed that EGCDNPs alone did not cause appreciable alterations in GP130 levels. EGCDNPs caused no significant change in GP130 levels in UM-UC-3 cells ($p = 0.6072$) (Fig. 7C) or in UM-UC-3R cells (Fig. 7D) ($p = 0.4493$). Next, we examined the efficiency of the EGCDNPs in delivering siRNA to UM-UC-3 and UM-UC-3R cells. Cells were exposed to EGCDNPs–siGP130 (4 µg/well siRNA) or 4 µg/well scrambled siRNA (siSC) loaded EGCDNPs. The silencing results showed that the siGP130–EGCDNPs performed equally as well as siGP130 – Lipofectamine RNAiMAX in knocking down GP130 levels in the UM-UC-3 cells ($p = 0.1919$) and in UM-UC-3R cells ($p = 0.6857$; Fig. 8A–D).

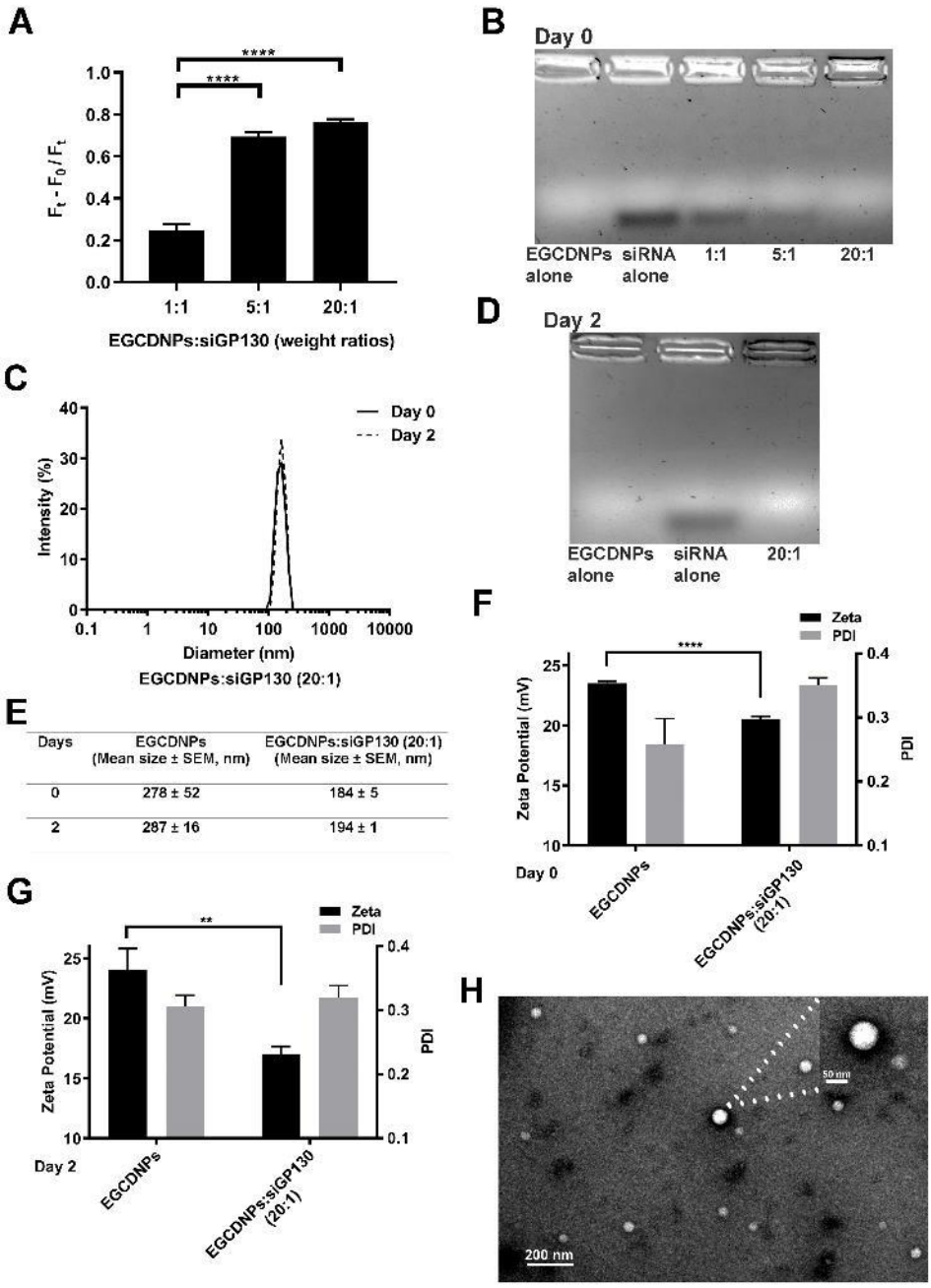

Fig. 6. Characterization of siGP130 EGCDNPs/EGCDNPs. siRNA binding to EGCDNPs was determined by measuring the reduction of PicoGreen fluorescence. Total fluorescence emitted by PicoGreen-bound siRNA alone (F_t) minus fluorescence emitted by PicoGreen incubated with EGCDNPs – siRNA complexes at EGCNDPs, siRNA mass ratios of 1:1, 5:1 and 20:1 (F_0), divided by the fluorescence emitted by PicoGreen-bound siRNA alone (F_t) (A). Agarose gel retardation data from EGCDNPs and EGCDNPs siGP130 complexes with mass ratios ranging from 1:1, 5:1 and 20:1 at day 0 (B), and at a mass ratio of 20:1 at day 2 (D). Stability of EGCDNPs/EGCDNPs

complexes between day 0 and day 2 determined by DLS (C, E). Zeta potential and PDI of the EGCDNPs and the EGCDNPs siGP130 complexes were determined by DLS at day 0 and day 2 indicating their stability (F, G). The morphology of siGP130 EGCDNPs at a mass ratio of 20:1 was determined by TEM (H). Two-way ANOVA and Sidak's multiple comparison tests were performed. Data are shown as mean ± SEM. ** represents $p < 0.01$ and **** $p < 0.0001$.

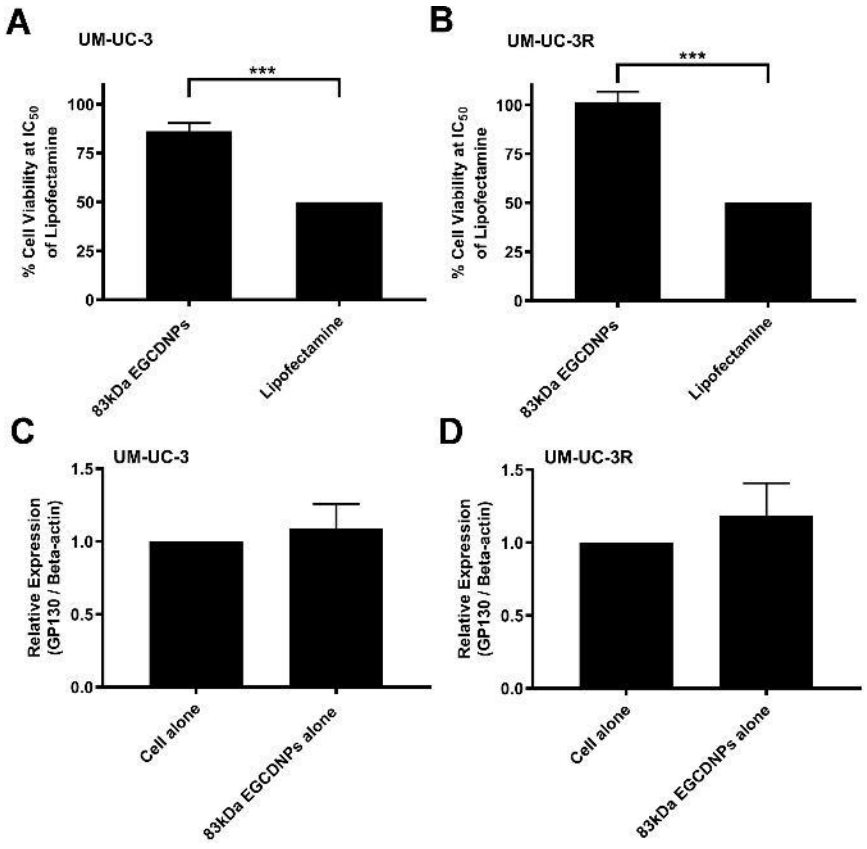

Fig. 7. EGCDNPs caused less toxicity than Lipofectamine and did not alter GP130 expression in bladder cancer cells. UM-UC-3 (A) and UM-UC-3R (B) bladder cancer cells were incubated with Lipofectamine 2000 or EGCDNPs and percent viability measured. UM-UC-3 (C) and UM-UC-3R (D) bladder cancer cells were incubated with EGCDNPs (40 µg/mL) and GP130 protein levels were measured and normalized against beta-actin. Data are shown as mean ± SEM. *** represents $p < 0.001$.

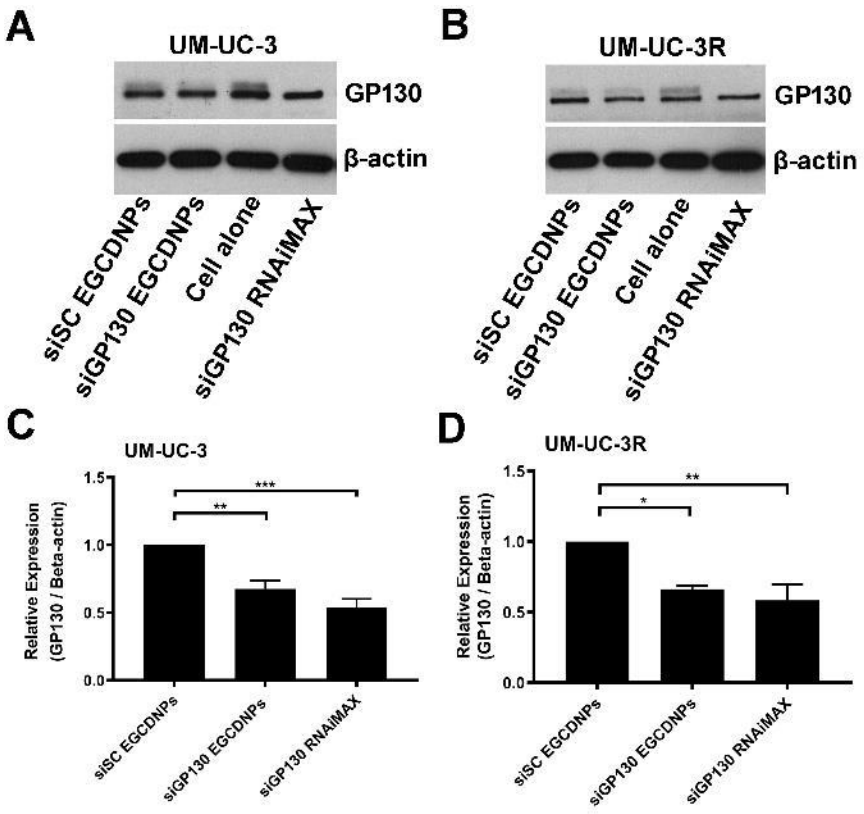

Fig. 8. siGP130 knockdown of GP130 protein using Lipofectamine and EGCDNPs delivery vehicles. The knockdown efficiency of the siGP130 EGCDNPs was compared with that of siGP130 Lipofectamine RNAiMAX by western blot in UM-UC-3 (A, C) and UM-UC-3R (B, D) cells. GP130 protein levels were measured and normalized against beta-actin. Data are shown as mean ± SEM. * represents $p < 0.05$, ** represents $p < 0.01$, and *** represents $p < 0.001$.

4. Discussion

Multiple reports have revealed that IL-6/GP130 pathways influence cell survival and proliferation [29-33]. Modulating IL-6/GP130 protein levels mediates cell death [34, 35]. Previously, we showed that inhibiting GP130 decreased cell proliferation and cell viability [17]. In this study, we observed that the decrease in cell viability was potentiated by combining GP130 protein knocked down with cisplatin, a DNA damaging agent (Fig. 2). Similar to our observations, others have reported that blocking other targets of the IL-6/GP130 pathway potentiates the actions of chemotherapeutic

agents. Long et al. showed in pancreatic ductal adenocarcinoma that IL-6R blockade in combination with chemotherapy potentiated apoptosis [36]. In addition, MEDI5117, an anti-IL-6 antibody, inhibited the expression of IL-6, leading to an enhanced *in vitro* killing of TF-1 human erythroleukemic cells, and in combination with chemotherapy enhanced anti-tumor activity in breast cancer [37]. Therefore, our goal was to demonstrate that, in addition to IL-6 and IL-6R, GP130 signaling also may play a role in apoptosis and DNA damage responses.

DNA damage was observed in our bladder cancer models subsequent to cisplatin treatment as shown by the increase in the number of DNA lesions. There was a significant increase in the number of DNA lesions with SC144 plus cisplatin co-treatment. This observation was more notable in the chemoresistant bladder cancer cells (i.e., UM-UC-3R) compared to the parental bladder cancer cells (i.e., UM-UC-3; Fig 3), suggesting a role of inhibiting GP130 signaling in sensitizing the resistant bladder cancer.

DSBs from cisplatin treatment results in the activation of the ATM signaling pathway [38, 39]. Specifically, the DSBs are followed by ATM recruitment, autophosphorylation, and phosphorylation of γH2AX [38, 40]. The detection of γH2AX is widely regarded as an indicator of the incidence of DSBs. In parental UM-UC-3 bladder cancer cells, a significant activation of pATM was observed upon sequential treatment with SC144 plus cisplatin whereas little effect was seen with either SC144 or cisplatin, alone (Fig. 4). The levels of γH2AX and pATM did not significantly change in parental and resistance cells upon SC144 treatment alone. Although cisplatin treatment alone altered the expression of pATM and γH2AX, the greatest changes in the levels of pATM and γH2AX occurred upon SC144 plus cisplatin co-treatment. The activation of pATM indicated that DNA damage was identified in parental and resistant cells.

Additionally, we suggest that another important DNA repair factor, Ku70, is involved in DSBs in bladder cancer. We have demonstrated for the first time that there is a significant correlation between GP130 and Ku70 protein levels in human bladder cancer tissues. Furthermore, using *in vitro* cancer cell models, we showed that down-regulating GP130 levels with SC144 resulted in the reduction of Ku70 protein levels (Fig. 4). SC144, a GP130 inhibitor, is a quinoxalinhydrazide derivative developed as a small molecular inhibitor that suppresses STAT3 signaling by inducing GP130 phosphorylation and by down-tuning GP130 glycosylation [41]. SC144 has anticancer activity in *in vitro* and in *in vivo* models of ovarian [41], pancreatic [42], bladder [17], prostate, breast, and lung cancers independent of p53, HER-2, or hormonal receptor status [43]. Our study shows that SC144 alone can down-regulate Ku70 expression in multiple cell types, including invasive bladder cancer cells (TCCSUP), breast cancer cells (MCF-7), and transformed embryonic kidney cells (HEK-293T), indicating that the GP130-regulated Ku70 down-regulation is shared by other tumor/cell types. The decreased Ku70 protein levels suggest that reduced c-NHEJ repair, may be mediated through GP130 inhibition, and may allow for improved responses to bladder cancer treatment. Similarly, Banerjee et al. reported enhanced c-NHEJ repair as a mechanism for induced chemoresistance in head and neck cancer [44]. In addition to the role of Ku70 in the initiation of the c-NHEJ repair pathway, several studies have demonstrated that Ku70 blocks Bax pro-apoptotic activity, and reduction/depletion of Ku70 levels promote cell death in human osteosarcoma and neuroblastoma [45, 46]. Free Bax, dissociated from the Ku70, translocates to the mitochondria, and initiates apoptotic cascades [47].

Although cisplatin alone did not alter the expression of Ku70 levels, a DNA damaging agent such as cisplatin was required to initiate apoptosis as was shown by the levels of cleaved caspase-3 expression (an apoptosis marker [48]). Higher levels of cleaved caspase-3 were observed following combined SC144 and cisplatin treatment than SC144 alone (Fig. 4A, 4F). SC144 alone

was unable to induce apoptosis above untreated conditions. Therefore, targeting Ku70 may be a feasible treatment modality in the presence of DNA damaging agents in bladder cancer.

The ultimate goal of our research is to develop potent and safe medicine to treat bladder cancer. We have incorporated nanoparticle technology to enhance the safety and delivery of cargo for intravesical administration to the bladder. In the past, we have used biocompatible materials such as poly(lactic-co-glycolic acid) (PLGA) or chitosan to deliver siRNA and found that PLGA, when coated with chitosan, achieved urothelium penetration in mouse bladders and human ureter [49]. Additionally, PLGA coated with chitosan induced potent siRNA gene silencing in mouse bladder models [17]. In the current study, we were interested in further enhancing intravesical delivery of genes and siRNAs to the bladder by devising a novel self-assembled approach in which a DOPE lipid was added into the positively charged chitosan derivative [N-(2-ethylamino)-6-O-glycolchitosan] EAGC to produce lipid-polymer hybrid nanoparticles (EGCDNPs). We revealed that an EGCDNP delivery system achieved an approximate 6-fold higher siRNA loading, when compared with the earlier study of chitosan-functionalized PLGA loaded with siGP130 [17]. Furthermore, data from TEM (Fig. 6H) showed that at an EGCDNPs:siRNA mass ratio of 20:1, EGCDNPs interact with anionic siGP130 to form condensed and spherical particles. The EGCDNPs–siRNA complex was stable over a two-day period without leaking free siRNA, indicating that EGCDNPs may be used as an effective carrier system for gene delivery. We also showed that this hybrid system is as efficacious as the commercial transfection agent–Lipofectamine in silencing GP130 protein, without the attendant cytotoxicity. In fact, numerous vectors such as Lipofectamine alone trigger alterations in signaling pathways [50], whereas our hybrid NPs are relatively non-toxic, allowing us to directly focus on cell signaling targets such as, GP130. Based on this investigation, we propose a new application for the utilization of this hybrid system; the exploration of the mechanism of GP130-enabled chemo-sensitization.

Our work suggests that GP130 elicits tumor progression [17], and may impact tumor heterogeneity by promoting low fidelity DNA NHEJ repair. We demonstrate an association of inhibition of GP130 signaling and Ku70 attenuation in various cancer cell models. Also, we generated a novel EAGC–DOPE hybrid lipid NP system that produces less toxicity than the traditional Lipofectamine vehicle, while still achieving similar levels of knockdown with GP130 siRNA. Ultimately, down-regulating GP130 sensitizes muscle invasive bladder cancer to cisplatin treatment by attenuating Ku70 expression and promoting apoptosis.

Acknowledgement

The authors would like to thank Dr. Jiangbing Zhou (Yale University) for his generosity in sharing resources during the project. This project was funded in part by a China's Scholarship Council fellowship (SH), a Qinghai Dimaer Tibetan Pharmaceutical Co., Ltd fellowship (GL), and by the Department of Defense (DoD) and the Congressionally Directed Medical Research Programs (CDMRP) grant W81XWH-19-PRCRP (DTM).

Reference

[1] H.B. Grossman, R.B. Natale, C.M. Tangen, V.O. Speights, N.J. Vogelzang, D.L. Trump, R.W. deVere White, M.F. Sarosdy, D.P. Wood, Jr., D. Raghavan, E.D. Crawford, Neoadjuvant chemotherapy plus cystectomy compared with cystectomy alone for locally advanced bladder cancer, The New England journal of medicine 349(9) (2003) 859-66.

[2] L. Galluzzi, L. Senovilla, I. Vitale, J. Michels, I. Martins, O. Kepp, M. Castedo, G. Kroemer, Molecular mechanisms of cisplatin resistance, Oncogene 31(15) (2012) 1869-83.

[3] E.R. Plimack, R.L. Dunbrack, T.A. Brennan, M.D. Andrake, Y. Zhou, I.G. Serebriiskii, M. Slifker, K. Alpaugh, E. Dulaimi, N. Palma, J. Hoffman-Censits, M. Bilusic, Y.N. Wong, A. Kutikov, R. Viterbo, R.E. Greenberg, D.Y. Chen, C.D. Lallas, E.J. Trabulsi, R. Yelensky, D.J. McConkey, V.A. Miller, E.A. Golemis, E.A. Ross, Defects in DNA Repair Genes Predict Response to Neoadjuvant Cisplatin-based Chemotherapy in Muscle-invasive Bladder Cancer, European urology 68(6) (2015) 959-67.

[4] D. Liu, E.R. Plimack, J. Hoffman-Censits, L.A. Garraway, J. Bellmunt, E. Van Allen, J.E. Rosenberg, Clinical Validation of Chemotherapy Response Biomarker ERCC2 in Muscle-Invasive Urothelial Bladder Carcinoma, JAMA Oncol 2(8) (2016) 1094-6.

[5] B.J. Sishc, A.J. Davis, The Role of the Core Non-Homologous End Joining Factors in Carcinogenesis and Cancer, Cancers (Basel) 9(7) (2017).

[6] M.Y. Teo, R.M. Bambury, E.C. Zabor, E. Jordan, H. Al-Ahmadie, M.E. Boyd, N. Bouvier, S.A. Mullane, E.K. Cha, N. Roper, I. Ostrovnaya, D.M. Hyman, B.H. Bochner, M.E. Arcila, D.B. Solit, M.F. Berger, D.F. Bajorin, J. Bellmunt, G. Iyer, J.E. Rosenberg, DNA Damage Response and Repair Gene Alterations Are Associated with Improved Survival in Patients with Platinum-Treated Advanced Urothelial Carcinoma, Clin Cancer Res 23(14) (2017) 3610-3618.

[7] N.C. Brissett, M.J. Martin, E.J. Bartlett, J. Bianchi, L. Blanco, A.J. Doherty, Molecular basis for DNA double-strand break annealing and primer extension by an NHEJ DNA polymerase, Cell Rep 5(4) (2013) 1108-20.

[8] E. Weterings, D.J. Chen, The endless tale of non-homologous end-joining, Cell Res 18(1) (2008) 114-24.

[9] R. Scully, A. Panday, R. Elango, N.A. Willis, DNA double-strand break repair-pathway choice in somatic mammalian cells, Nat Rev Mol Cell Biol 20(11) (2019) 698-714.

[10] A. Rivera-Calzada, L. Spagnolo, L.H. Pearl, O. Llorca, Structural model of full-length human Ku70-Ku80 heterodimer and its recognition of DNA and DNA-PKcs, EMBO Rep 8(1) (2007) 56-62.

[11] V.L. Fell, C. Schild-Poulter, The Ku heterodimer: function in DNA repair and beyond, Mutat Res Rev Mutat Res 763 (2015) 15-29.

[12] S.H. Kim, D. Kim, J.S. Han, C.S. Jeong, B.S. Chung, C.D. Kang, G.C. Li, Ku autoantigen affects the susceptibility to anticancer drugs, Cancer research 59(16) (1999) 4012-7.

[13] M.F. Chen, P.Y. Lin, C.F. Wu, W.C. Chen, C.T. Wu, IL-6 expression regulates tumorigenicity and correlates with prognosis in bladder cancer, PloS one 8(4) (2013) e61901.

[14] J. Mauer, J.L. Denson, J.C. Bruning, Versatile functions for IL-6 in metabolism and cancer, Trends Immunol 36(2) (2015) 92-101.

[15] Z.T. Schafer, J.S. Brugge, IL-6 involvement in epithelial cancers, The Journal of clinical investigation 117(12) (2007) 3660-3.

[16] R. Salgado, S. Junius, I. Benoy, P. Van Dam, P. Vermeulen, E. Van Marck, P. Huget, L.Y. Dirix, Circulating interleukin-6 predicts survival in patients with metastatic breast cancer, International journal of cancer. Journal international du cancer 103(5) (2003) 642-6.

[17] D.T. Martin, H. Shen, J.M. Steinbach-Rankins, X. Zhu, K.K. Johnson, J. Syed, W.M. Saltzman, R.M. Weiss, Glycoprotein-130 Expression Is Associated with Aggressive Bladder Cancer and Is a Potential Therapeutic Target, Molecular cancer therapeutics 18(2) (2019) 413-420.

[18] Y. Chen, F. Zhang, Y. Tsai, X. Yang, L. Yang, S. Duan, X. Wang, P. Keng, S.O. Lee, IL-6 signaling promotes DNA repair and prevents apoptosis in CD133+ stem-like cells of lung cancer after radiation, Radiat Oncol 10 (2015) 227.

[19] S. Duan, Y. Tsai, P. Keng, Y. Chen, S.O. Lee, Y. Chen, IL-6 signaling contributes to cisplatin resistance in non-small cell lung cancer via the up-regulation of anti-apoptotic and DNA repair associated molecules, Oncotarget 6(29) (2015) 27651-60.

[20] S.S. Tseng-Rogenski, Y. Hamaya, D.Y. Choi, J.M. Carethers, Interleukin 6 alters localization of hMSH3, leading to DNA mismatch repair defects in colorectal cancer cells, Gastroenterology 148(3) (2015) 579-89.

[21] S. GuhaSarkar, R. Banerjee, Intravesical drug delivery: Challenges, current status, opportunities and novel strategies, J Control Release 148(2) (2010) 147-59.

[22] L. Denis, Anaphylactic reactions to repeated intravesical instillation with cisplatin, Lancet 1(8338) (1983) 1378-9.

[23] M.I. Simao Carlos, K. Zheng, N. Garrett, N. Arifin, D.G. Workman, I. Kubajewska, A.A. Halwani, J. Moger, Q. Zhang, A.G. Schatzlein, I.F. Uchegbu, Limiting the level of tertiary amines on polyamines leads to biocompatible nucleic acid vectors, International journal of pharmaceutics 526(1-2) (2017) 106-124.

[24] P.A. Humphrey, H. Moch, A.L. Cubilla, T.M. Ulbright, V.E. Reuter, The 2016 WHO Classification of Tumours of the Urinary System and Male Genital Organs-Part B: Prostate and Bladder Tumours, European urology 70(1) (2016) 106-119.

[25] X. Li, S. He, Y. Tian, R.M. Weiss, D.T. Martin, Synergistic inhibition of GP130 and ERK signaling blocks chemoresistant bladder cancer cell growth, Cell Signal 63 (2019) 109381.

[26] D.T. Martin, C.J. Hoimes, H.Z. Kaimakliotis, C.J. Cheng, K. Zhang, J. Liu, M.A. Wheeler, W.K. Kelly, G.N. Tew, W.M. Saltzman, R.M. Weiss, Nanoparticles for urothelium penetration and delivery of the histone deacetylase inhibitor belinostat for treatment of bladder cancer, Nanomedicine 9(8) (2013) 1124-34.

[27] H.L. Smith, H. Southgate, D.A. Tweddle, N.J. Curtin, DNA damage checkpoint kinases in cancer, Expert Rev Mol Med 22 (2020) e2.
[28] L.J. Mah, A. El-Osta, T.C. Karagiannis, gammaH2AX: a sensitive molecular marker of DNA damage and repair, Leukemia 24(4) (2010) 679-86.
[29] K.H. Shain, D.N. Yarde, M.B. Meads, M. Huang, R. Jove, L.A. Hazlehurst, W.S. Dalton, Beta1 integrin adhesion enhances IL-6-mediated STAT3 signaling in myeloma cells: implications for microenvironment influence on tumor survival and proliferation, Cancer research 69(3) (2009) 1009-15.
[30] N. Juge-Morineau, S. Francois, D. Puthier, A. Godard, R. Bataille, M. Amiot, The gp 130 family cytokines IL-6, LIF and OSM but not IL-11 can reverse the anti-proliferative effect of dexamethasone on human myeloma cells, Br J Haematol 90(3) (1995) 707-10.
[31] D. Chauhan, P. Pandey, T. Hideshima, S. Treon, N. Raje, F.E. Davies, Y. Shima, Y.T. Tai, S. Rosen, S. Avraham, S. Kharbanda, K.C. Anderson, SHP2 mediates the protective effect of interleukin-6 against dexamethasone-induced apoptosis in multiple myeloma cells, The Journal of biological chemistry 275(36) (2000) 27845-50.
[32] P.M. Voorhees, Q. Chen, G.W. Small, D.J. Kuhn, S.A. Hunsucker, J.A. Nemeth, R.Z. Orlowski, Targeted inhibition of interleukin-6 with CNTO 328 sensitizes pre-clinical models of multiple myeloma to dexamethasone-mediated cell death, Br J Haematol 145(4) (2009) 481-90.
[33] J. Bollrath, T.J. Phesse, V.A. von Burstin, T. Putoczki, M. Bennecke, T. Bateman, T. Nebelsiek, T. Lundgren-May, O. Canli, S. Schwitalla, V. Matthews, R.M. Schmid, T. Kirchner, M.C. Arkan, M. Ernst, F.R. Greten, gp130-mediated Stat3 activation in enterocytes regulates cell survival and cell-cycle progression during colitis-associated tumorigenesis, Cancer cell 15(2) (2009) 91-102.
[34] A. Demartis, F. Bernassola, R. Savino, G. Melino, G. Ciliberto, Interleukin 6 receptor superantagonists are potent inducers of human multiple myeloma cell death, Cancer research 56(18) (1996) 4213-8.

[35] M. Hatting, M. Spannbauer, J. Peng, M. Al Masaoudi, G. Sellge, Y.A. Nevzorova, N. Gassler, C. Liedtke, F.J. Cubero, C. Trautwein, Lack of gp130 expression in hepatocytes attenuates tumor progression in the DEN model, Cell death & disease 6 (2015) e1667.
[36] K.B. Long, G. Tooker, E. Tooker, S.L. Luque, J.W. Lee, X. Pan, G.L. Beatty, IL6 Receptor Blockade Enhances Chemotherapy Efficacy in Pancreatic Ductal Adenocarcinoma, Molecular cancer therapeutics 16(9) (2017) 1898-1908.
[37] H. Zhong, A. Davis, M. Ouzounova, R.A. Carrasco, C. Chen, S. Breen, Y.S. Chang, J. Huang, Z. Liu, Y. Yao, E. Hurt, J. Moisan, M. Fung, D.A. Tice, S.G. Clouthier, Z. Xiao, M.S. Wicha, H. Korkaya, R.E. Hollingsworth, A Novel IL6 Antibody Sensitizes Multiple Tumor Types to Chemotherapy Including Trastuzumab-Resistant Tumors, Cancer research 76(2) (2016) 480-90.
[38] T. Clouaire, A. Marnef, G. Legube, Taming Tricky DSBs: ATM on duty, DNA repair 56 (2017) 84-91.
[39] J.H. Jeon, S.K. Kim, H.J. Kim, J. Chang, C.M. Ahn, Y.S. Chang, Insulin-like growth factor-1 attenuates cisplatin-induced gammaH2AX formation and DNA double-strand breaks repair pathway in non-small cell lung cancer, Cancer letters 272(2) (2008) 232-41.
[40] L. Centurione, F.B. Aiello, DNA Repair and Cytokines: TGF-beta, IL-6, and Thrombopoietin as Different Biomarkers of Radioresistance, Front Oncol 6 (2016) 175.
[41] S. Xu, F. Grande, A. Garofalo, N. Neamati, Discovery of a novel orally active small-molecule gp130 inhibitor for the treatment of ovarian cancer, Molecular cancer therapeutics 12(6) (2013) 937-49.
[42] X. Chen, J. Tian, G.H. Su, J. Lin, Blocking IL-6/GP130 Signaling Inhibits Cell Viability/Proliferation, Glycolysis, and Colony Forming Activity in Human Pancreatic Cancer Cells, Curr Cancer Drug Targets 19(5) (2019) 417-427.

[43] C. Plasencia, F. Grande, T. Oshima, X. Cao, R. Yamada, T. Sanchez, F. Aiello, A. Garofalo, N. Neamati, Discovery of a novel quinoxalinhydrazide with a broad-spectrum anticancer activity, Cancer biology & therapy 8(5) (2009) 458-65.

[44] R. Banerjee, N. Russo, M. Liu, V. Basrur, E. Bellile, N. Palanisamy, C.S. Scanlon, E. van Tubergen, R.C. Inglehart, T. Metwally, R.S. Mani, A. Yocum, M.K. Nyati, R.M. Castilho, S. Varambally, A.M. Chinnaiyan, N.J. D'Silva, TRIP13 promotes error-prone nonhomologous end joining and induces chemoresistance in head and neck cancer, Nature communications 5 (2014) 4527.

[45] M. Hada, C. Subramanian, P.C. Andrews, R.P. Kwok, Cytosolic Ku70 regulates Bax-mediated cell death, Tumour Biol 37(10) (2016) 13903-13914.

[46] A.D. Amsel, M. Rathaus, N. Kronman, H.Y. Cohen, Regulation of the proapoptotic factor Bax by Ku70-dependent deubiquitylation, Proceedings of the National Academy of Sciences of the United States of America 105(13) (2008) 5117-22.

[47] S. Pucci, P. Mazzarelli, F. Sesti, D.A. Boothman, L.G. Spagnoli, Interleukin-6 affects cell death escaping mechanisms acting on Bax-Ku70-Clusterin interactions in human colon cancer progression, Cell cycle 8(3) (2009) 473-81.

[48] A.G. Porter, R.U. Janicke, Emerging roles of caspase-3 in apoptosis, Cell death and differentiation 6(2) (1999) 99-104.

[49] D.T. Martin, J.M. Steinbach, J. Liu, S. Shimizu, H.Z. Kaimakliotis, M.A. Wheeler, A.B. Hittelman, W. Mark Saltzman, R.M. Weiss, Surface-modified nanoparticles enhance transurothelial penetration and delivery of survivin siRNA in treating bladder cancer, Molecular cancer therapeutics 13(1) (2014) 71-81.

[50] X. Guo, H. Wang, Y. Li, X. Leng, W. Huang, Y. Ma, T. Xu, X. Qi, Transfection reagent Lipofectamine triggers type I interferon signaling activation in macrophages, Immunol Cell Biol 97(1) (2019) 92-96.

Supplementary Data

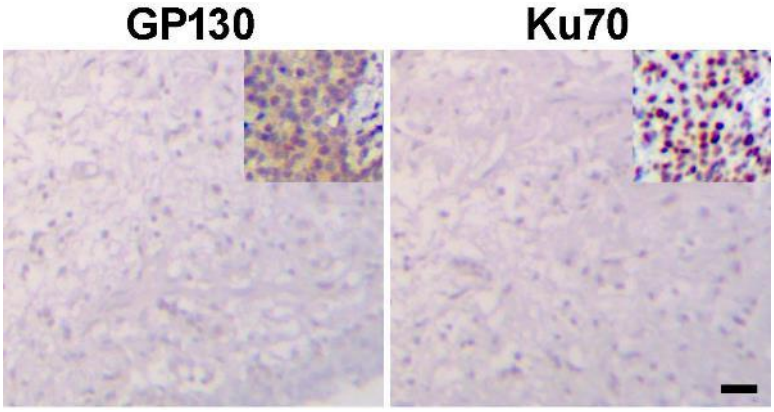

Fig. S1. GP130 and Ku70 levels of expression in normal human bladder specimens. Immunohistochemistry was performed on normal bladder tissue (cancer adjacent) for GP130 (A) and Ku70 (B). Scale bar = 10 µm. Insets are positive control bladder cancer specimens.